Mechanical Performance and Safety Evaluation of Connection Nodes in Prefabricated Assembled Structures

Jipeng Liu

Department of Civil Engineering, Henan University of Engineering, Zhengzhou 451191, Henan, China

Corresponding author: Jipeng Liu (e-mail: 13253582186@163.com)

ABSTRACT The long-term reliability of communication infrastructures, antenna supporting systems, and integrated engineering platforms in Electromagnetic Waves, Antennas and Propagation increasingly depends on the mechanical stability and safety of their structural connection components. To address the difficulty of quantitatively evaluating the stress behavior and safety performance of prefabricated assembled joints, this study proposes a comprehensive framework integrating structural parameter modeling, finite element analysis (FEA), mechanical performance extraction, and multi-index safety assessment. A three-dimensional numerical model is established to characterize stress distribution, deformation evolution, stiffness degradation, and failure mechanisms under combined loading conditions. Based on the simulated mechanical responses, ultimate bearing capacity, equivalent stiffness retention coefficient, and ductility coefficient are extracted and incorporated into a normalized weighted evaluation model to construct a comprehensive safety index for quantitative reliability assessment. Experimental results show that under C50 concrete, HRB500 reinforcement, and a sleeve length of 180 mm, the connection node achieves an ultimate bearing capacity of 356 kN, an equivalent stiffness retention coefficient of 0.82, a ductility coefficient of 3.59, and an overall safety index exceeding 0.90, demonstrating excellent structural performance. The proposed framework provides a robust methodology for structural reliability evaluation and engineering optimization of complex load-bearing systems, with potential applications in antenna supporting structures, communication infrastructure design, and mechanically integrated platforms associated with Electromagnetic Waves, Antennas and Propagation.

INDEX TERMS finite element analysis, structural reliability, prefabricated connection nodes, antenna supporting structures

I. INTRODUCTION

PREFABRICATED assembly structures have become a cornerstone of contemporary industrialized construction and green building initiatives, leveraging high-performance fiber morphology and technical reinforcements to achieve exceptional construction efficiency, resource optimization, and structural quality. The integration of three-dimensional architectures within these modular components further enhances the mechanical durability and material sustainability of the final assembly. Being the most important links of components, the mechanical properties of nodes directly influence the load-bearing capacity of the whole structure, the distribution of stiffness, and seismic performance [1-2]. A systematic study of the mechanical behavior and safety evaluation of nodes can provide a theoretical basis for structural design, reduce safety risks during construction and use, and improve the reliability and durability of prefabricated buildings [3].

The force transmission at connection nodes is complex, with significant local stress concentration. The deformation coordination of component joints is difficult to quantify, and the synergistic stress of steel reinforcement and concrete exhibits nonlinear and time-varying characteristics [4-5]. Nodes used under vertical and horizontal loads have degradation of stiffness, plastic formation and several failure modes. The current design techniques and safety requirements are mainly based on single indicators or even empirical formulas, and therefore, they are not reliable to represent the overall stress state and safety reserve of nodes in complex working conditions [6-7].

Methods that are available consist of finite element analysis, node loading tests, and the theoretical mechanical models. The three-dimensional stress and deformation can be simulated using the finite element analysis (FEA), but interface treatment and material nonlinearity assumptions are not adequate to capture local failure properties [8-9]. Loading tests offer nodal mechanical information, and the samples are constrained by component specifications and cost, so it is not within the full parameter range [10-11]. Theoretical mechanics analysis may solve the correlation between nodal stress and deformation, yet it is not that accurate in computing under complex geometry and nonlinear load conditions [12-13]. Although such techniques offer fundamental assistance, systemic interaction in relation to nodal stress reaction and multi-index safety analysis does not exist, so no adequate precision in nodal safety analysis is achieved [14-15]. This study attempts to achieve comprehensive safety assessment through node parameter modeling, three-dimensional finite element simulation, and performance index extraction to address the issues of complex stress distribution at nodes and insufficient performance-based safety evaluation in fiber-reinforced composite structures. By integrating technical distribution into the mechanical modeling process, the research provides a multi-scale quantitative framework for evaluating the structural integrity of advanced engineering assemblies. The study evaluates nodal performance by partitioning the structure into three distinct functional regions: the core stress zone, the force transmission zone, and the constraint boundary zone. Further, a mechanical analysis model is formulated, where the nodal geometry, material and connection parameters are incorporated in the calculation. Following this, modeling of stress-deformation-plastic zone development at the node subjected to vertical dead load and horizontal cyclic load is carried out through finite element analysis to obtain the bearing capacity, stress-siffth degradation, and ductile indices. In the end, a weighted safety assessment model with multiple indices of safety is built. The extreme values obtaine from the mechanica functioning of the node is standardized and weights assigned to transform the mechanical functioning into a quantitative comprehensive safety index for quantitative classification and assessment of node safety functioning. This gives a measurable basis of design optimization decision making and engineering applications, and it gives a complete verification with the total safety index achieved after later experiments.

II. METHODS

STRESS MECHANISM AND STRUCTURAL PARAMETER MODELING OF CONNECTION NODES

In prefabricated assembled structures, connection nodes are key areas for force transmission and deformation coordination between components. Their stress state is determined by the node geometry, reinforcement arrangement, concrete properties, and connection method [16-17]. To accurately describe the mechanical behavior of nodes, this study divides nodes into core stress zones, connection force transmission zones, and constraint boundary zones, and establishes a node stress analysis model based on structural mechanics principles. The core stress zone of a node mainly bears the transmission of shear force and bending moment, and its stress can be calculated through the normal stress and shear stress within the node section [18-19]. The axial stress σ_n of a node under the combined action of vertical load P_v and horizontal load P_h can be expressed as:

$$\sigma_n = \frac{P_v + \beta P_h}{A_c} + \alpha \frac{M_v + M_h}{W} \tag{1}$$

In Formula (1), σ_n represents the axial stress of the node section; β is the axial stress distribution coefficient of the horizontal load, reflecting the proportion of the horizontal load in the axial stress of the node; M_v is the bending moment caused by the vertical load; M_h is the bending moment caused by the horizontal load; A_c is the area of the core concrete section of the node; W is the bending resistance moment of the section; α is the bending moment distribution coefficient.

The shear stress τ of the node can be determined by the relationship between the shear force V and the cross-sectional area A_s in the connection force transmission zone:

$$\tau = \frac{V}{A_s} \tag{2}$$

In Formula (2), τ is the shear stress of the node; V is the shear force of the node section; A_s is the effective cross-sectional area of the connection force transmission zone.

The node stiffness is defined as the ratio of the node load to the deformation, and is defined as:

$$K_n = \frac{\Delta P}{\Delta \delta} \tag{3}$$

In Formula (3), K_n represents the equivalent stiffness of the node; ΔP is the load increment; and $\Delta\delta$ is the corresponding displacement increment.

To systematically reflect the influence of node parameters on mechanical properties, this study establishes a node structural parameter system, covering geometric parameters, material parameters, and connection method parameters, forming a standard input dataset for node modeling. Table 1 lists the typical beam-column node modeling parameters used in this paper, including key parameters such as core area dimensions, cross-sectional dimensions, steel bar yield strength, and sleeve connection length, providing a unified parameter basis for the node mechanical model.

Table 1 lists parameters covering the core influencing factors of node mechanical performance. Geometric dimensions control the stress distribution range of the node; material parameters determine the node's ultimate bearing capacity and ductility; connection method parameters reflect the node's load transfer efficiency and local stress control. Through this parameter system, the theoretical stress analysis and finite element modeling of the node form a unified standard at the input level, realizing a systematic modeling process from node structural characteristics to mechanical response.

TABLE 1. Modeling parameters for connection nodes in prefabricated assembled structures

Parameter Category	Parameter Name	Value Range	Unit	Description
Geometric Parameters	Core Zone Dimension of Joint	300–600	mm	Region where stresses in the joint are most concentrated
	Beam Section Height	400–800	mm	Influences bending moment distribution
	Column Section Width	500–900	mm	Determines shear force transfer capacity
Material Parameters	Concrete Strength Grade	C30–C60	–	Determines compressive performance
	Reinforcement Yield Strength	400–500	MPa	Influences joint ductility and load-bearing capacity
Connection Parameters	Sleeve Connection Length	120–220	mm	Controls load transfer efficiency of the joint
	Reinforcement Spacing	100–200	mm	Adjusts shear load-bearing capacity of the joint

SIMULATION METHOD OF MECHANICAL RESPONSE OF CONNECTION NODES BASED ON FINITE ELEMENT ANALYSIS

This paper works with the finite element analysis approach to create a three-dimensional numerical model of the node to precisely simulate the mechanical response of prefabricated precast beam-column connection node with various load configurations [20-21]. The model of the concrete region is made in solid elements to reflect the nonlinear compressive behavior of material and crack development characteristics, and the model of reinforcing steel is made in embedded elements to reflect synergistic stress interaction between reinforcing steel and concrete [22-23]. Contacts between a node core region and force transmission region are set by contact elements. It regulates the transmission of shear forces and the concentration of local stresses, based on the coefficient of friction and contact hardness, achieving accurate reproduction of the mechanism of force on the node connection [24-25].

The loading plan is determined to be a mixture of both vertical and horizontal loading, which is executed in gradual successions, that makes the node experience the elastic, plastic, and ultimate failure stages [26-27].

The finite element analysis provides the nonlinear relationship between displacement of nodes and load, and the node stress state is presented as the following formula:

$$\sigma_{ij} = D_{ijkl} \cdot \epsilon_{kl} \tag{4}$$

In Formula (4), σ_{ij} is the stress tensor within the node element; ϵ_{kl} is the strain tensor; and D_{ijkl} is the material constitutive matrix, reflecting the nonlinear elastoplastic characteristics of concrete and steel reinforcement.

The development of the plastic zone and material nonlinearity in the concrete phase of the node is determined by the Concrete Damaged Plasticity (CDP) model, which accounts for the quasi-brittle nature of concrete by incorporating different yield surfaces for tension and compression [28-29]. The plastic strain ϵ_p of the node can be expressed as:

$$\epsilon_p = \sqrt{\frac{2}{3}\left[(\epsilon_1 - \epsilon_2)^2 + (\epsilon_2 - \epsilon_3)^2 + (\epsilon_3 - \epsilon_1)^2\right]} \tag{5}$$

In Formula (5), ϵ_1, ϵ_2, and ϵ_3 are the principal strains of the node element, and ϵ_p describes the degree of plastic development in the core region of the node, used for subsequent performance index extraction. This paper uses modeled and calculated stress, displacement and plastic zone development of a node at various loads as input data to extract structural performance indicators. The framework of the proposed nodal mechanical response simulation method is shown in Figure 1. The proposed framework employs finite element analysis (FEA) to form a logical relationship between the nodal parameter modeling layer, finite element mechanical analysis layer, and the stress-displacement evolution output layer, and provides a means for implementing the method of mapping nodal mechanical response data to define structural safety evaluation indicators.

The relationship between the modules is depicted in Figure 1 that demonstrates the impact of node geometry and material parameter on the results of the finite element calculation and how the key performance indicators (stress, plastic strain, displacement, stiffness) can be deployed in the safety evaluation layer to have a complete technical path to quantitative analysis of node structural performance. This framework is an organic connection of calculating mechanical behavior of the node, extracting the evaluation features of evolution, and the analysis of the model of safety evaluation, which realizes the systematic analysis between the simulation and evaluation.

EXTRACTION AND QUANTIFICATION METHOD OF NODE MECHANICAL PERFORMANCE INDICATORS

Based on the data of node stress, displacement, and plastic zone evolution obtained from finite element simulation, a quantitative evaluation system for node mechanical performance is constructed to realize the quantitative analysis of the load-bearing, deformation, and stability performance of node structures [30-31]. The ultimate bearing capacity P_u of a node is determined by the load-displacement curve.

$$P_u = \max(P(\delta)) \tag{6}$$

In Formula (6), $P(\delta)$ represents the load response of the node under different displacements δ. The yield displacement δ_y of the node is calculated based on the intersection of the end point of the elastic stage and the initial stiffness line to characterize the starting position of the node entering the plastic stage. The ductility coefficient μ of the node is calculated by the ratio of the ultimate displacement to the yield displacement, and the formula is:

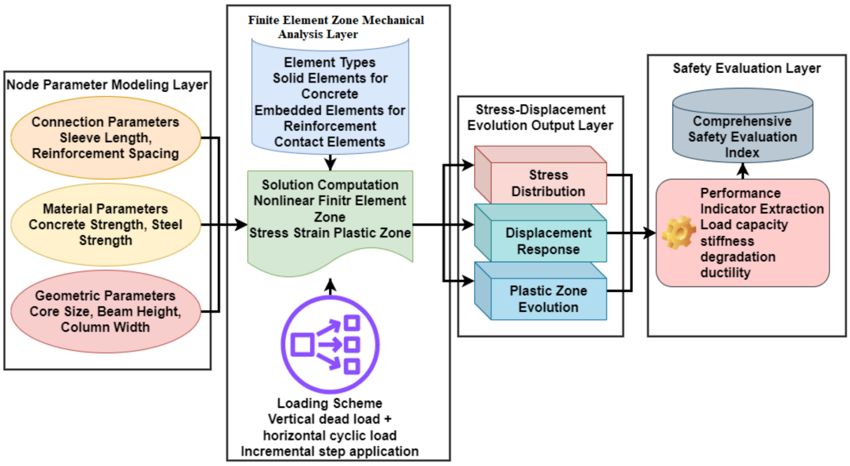

FIGURE 1. Framework of simulation method for mechanical response of connection nodes in prefabricated assembled structures

$$\mu = \frac{\delta_u}{\delta_y} \tag{7}$$

In Formula (7), δ_u represents the ultimate displacement of the node, and μ is used to reflect the deformation capacity and energy dissipation characteristics of the node in the plastic stage. The equivalent stiffness degradation coefficient K_{eq} is calculated based on the local slope of the load-displacement curve at different loading stages, and its expression is:

$$K_{\text{eq}} = \frac{K_n}{\Delta\delta} \tag{8}$$

In Formula (8), K_n is the load increment; $\Delta\delta$ is the corresponding displacement increment, and the unit is mm. K_{eq} reflects the attenuation law of node stiffness with the increase of load. The stress concentration coefficient C_s of the node core area is calculated by the ratio of the maximum stress $\sigma_{\max}$ to the average stress σ_{avg} of the key element of the node:

$$C_s = \frac{\sigma_{\max}}{\sigma_{\text{avg}}} \tag{9}$$

In Formula (9), C_s indicates the degree of non-uniformity of local stress distribution of the node, providing a reference for safety evaluation. The above-mentioned index extraction method forms a set of node structural performance characteristics, which can be used for the calculation of subsequent safety evaluation models, realizing the mapping and transformation of node mechanical behavior into safety quantification indicators.

CONSTRUCTION OF MULTI-INDICATOR COMPREHENSIVE SAFETY EVALUATION MODEL FOR CONNECTION NODES

Based on the quantitative results of structural performance indicators, a safety evaluation model for connection nodes of prefabricated assembled structures is constructed to achieve a quantitative mapping of node stress performance to a safe state [32-33]. The model selects the node ultimate bearing capacity P_u, the equivalent stiffness degradation coefficient K_{eq}, and the node ductility coefficient μ as the main performance indicators. The dimensionless evaluation value S_i of each indicator is obtained through standardization:

$$S_i = \frac{X_i - X_{\min}}{X_{\max} - X_{\min}} \tag{10}$$

In Formula (10), X_i represents the actual value of the i-th structural performance indicator of the node, with the same unit as the original indicator; $X_{\min}$ and $X_{\max}$ represent the minimum and maximum values of the indicator within the research sample range, respectively; S_i is the standardized indicator value, used to eliminate the influence of different dimensions on the comprehensive evaluation. A weighting coefficient w_i is introduced for each indicator to form the node comprehensive safety evaluation index I_s.

$$I_s = \sum_{i=1}^{n} w_i S_i \tag{11}$$

In Formula (11), n represents the number of performance indicators; w_i is the weight of the i-th indicator, with a value range of 0–1, satisfying $\Sigma_{i=1}^{n} w_i = 1$; I_s is between 0 and 1, and the closer the value is to 1, the better the safety performance of the node. The evaluation model achieves a comprehensive judgment on the overall structural safety status of the node by weighted summing of the standardized values of the node bearing capacity margin, stiffness retention coefficient, and ductility parameter.

In the process of model implementation, the node bearing capacity curve and displacement response curve obtained by finite element simulation are first processed to extract the ultimate load, yield displacement, and ultimate displacement data; then the equivalent stiffness degradation curve and ductility coefficient are calculated to form a performance indicator dataset; then each indicator is standardized and the weighting coefficient ω_i is determined through the Analytic Hierarchy Process (AHP) to minimize subjectivity in the importance assessment of the project, and finally the node comprehensive safety evaluation index is calculated [34-35]. This method ensures a continuous mapping from single mechanical response to overall safety level, so that the node stress analysis results directly reflect the structural safety level, and provides a quantitative basis for safety comparison under different node construction and material conditions.

The quantitative safety levels are defined based on the distribution of index I_s: Grade I (High Safety, $I_s \geq 0.90$), Grade II (Medium-High Safety, $0.85 \leq I_s < 0.90$), Grade III (Medium Safety, $0.80 \leq I_s < 0.85$), and Grade IV (Low Safety, $I_s < 0.80$), which aligns with the performance-based design requirements for prefabricated structures in China.

III. EXPERIMENT AND VERIFICATION

EXPERIMENTAL SETUP AND WORKING CONDITION DESIGN

The study object in the experiment is a typical precast beam-column joint, and a three-dimensional finite element model is built to recreate the mechanical behaviour of the joint under the real-life engineering stress condition. The concrete is modeled by solid elements, and the nonlinear constitutive relation of the material is based on the strength grade of C30-C60. The simulated synergistic stress effect between the steel reinforcement and the concrete is achieved by making use of embedded elements. The contact elements are defined with a "Hard" contact in the normal direction and a "Penalty" friction coefficient of 0.4 in the tangential direction to simulate the bond-slip behavior. Geometric parameters are founded on real engineering design information: beam height (400-800 mm), column cross-section width (500-900 mm), sleeve connection length (120-220 mm), steel reinforcement spacing (100-200 mm). The reinforcing steel strength is chosen to be 400-500 MPa, and the characteristics of concrete material are given by the engineering requirements and the material test report accessible in the open market.

The loading regime is determined to be the combination of vertical dead loading and horizontal cyclic loading where the loading is increased in phases. The node responses to the stress, strain and displacement stages are measured at various stages. The vertical load applies the force of the weight of the beams and columns themselves and the live load effect, whereas the horizontal cyclic load applies to the effect of earthquakes and wind loads. Static equilibrium iterations are performed after each stage of load application to ensure the convergence of the finite element model of the nodes. Displacement boundary conditions are applied to the bottom of the column by constraining all six degrees of freedom ($U_x = U_y = U_z = UR_x = UR_y = UR_z = 0$) to simulate a fixed support condition. The data gathered in the process of simulation comprises a node response curve to bearing capacity, evolution of node stiffness, core area stress distribution and plastic zone formation, which forms a platform upon which performance index would be extracted later.

To be sure about the authenticity and reproducibility of the experimental data, the material and geometry parameters of the nodes are determined by engineering design data that is publicly available and the standards of material testing. Parameters of concrete materials are determined according to the Standard of Testing Mechanical Properties of Ordinary Concrete (GB/T 50081-2019), and steel reinforcement material parameters according to the Standard of Steel reinforced concrete (GB 1499-2024). Parameters of the node geometry and connection method are based on the real construction data of large prefabricated modular building projects that have been built in China. Finite element analysis is performed using Abaqus software, with mesh generation controlled at 20–30 mm element size in the core stress zone and 30–40 mm element size in the load-transfer zone to ensure a balance between analytical accuracy and computational efficiency. The experimental data collection includes the load-displacement response of the nodes during the elastic, plastic development, and failure stages, as well as the stress distribution and displacement in the node core and connection areas. This data gathering procedure builds a complete database of node stress reactions, and enables a unitary input criterion of mining the structural performance indicators and building safety assessment paradigms.

LOAD-BEARING CAPACITY OF NODES

The load-displacement response results of the nodes of the prefabricated assembled structure connection made of the finite element are processed to explore the load transfer and resistance capacity of the node at various stages of the stress. Stress distribution patterns of core region and the general displacement response in response to each loading factor are obtained, thus identifying both the yield load and ultimate load as well as the respective values of displacement at the nodes. Comparison and analysis of the load-bearing behavior in the case of monotonic and cyclic loads on different node models make it possible to obtain the effects of the parameters of the node construction and material strength on the load-bearing capacity. In order to produce the simulated load-displacement curves, curves are normalized, and the curve of the evolution of the node load bearing capacity is plotted as in Figure 2. This paper establishes five categories of beam-column node models to arrange a comprehensive study on the impact of different parameters on mechanical properties. Model A serves as the baseline node, employing traditional materials and construction methods, with specific dimensions set at a beam section height of 600 mm, a column section width of 700 mm, and a sleeve connection length of 150 mm to represent a standard engineering configuration. In Model B, the concrete strength, the steel reinforcement strength, and the sleeve length are all well optimized (C50, HRB500 (Hot-rolled Ribbed Bars), and 180 mm, respectively), whereas in Model C, Model D, and Model E, only one need is fulfilled (respectively, the concrete strength, the steel reinforcement strength, and the sleeve length, to C50, HRB500, and 180 mm, respectively). Through comparing these five models, it is possible to quantitatively determine the independent and synergistic contributions to the load-bearing capacity, stiffness degradation, and ductility of the node using the contribution of the material strength, the reinforcement detail, and the connection length.

The curve in Figure 2 (a) indicates that the process of stress of the node is divided into the elastic stage, elastoplastic stage, and the failure stage. The point of the inflection can be seen in the yield point and then goes on to rise in load up to the peak point in the curve. The curve also decays slowly towards the end. As can be seen from Figure 2(b), the ultimate load of the node using high-strength materials and reasonable reinforcement reaches 356 kN, which is about 18% higher than that of the reference node. The great reason of this disparity is due to synergistic impact of high strength concrete and steel reinforcement, which enhances compressive and tensile strength of core region of the node. Decent structural design of the sleeve connection area allows transmitting of the forces efficiently, postponing the core concrete crushing and the yielding process of the steel reinforcement. The load gain period at the node is steady, and then the node reaches its final load that is reflective of the good stress performance of the node and has a bearing capacity reserve.

NODAL STIFFNESS DEGRADATION CHARACTERISTICS

To clarify the evolution law of the deformation resistance of connection nodes in prefabricated assembled structures throughout the entire loading process, the secant stiffness of nodes under each loading level is calculated based on the load-displacement data output from the finite element simulation, and degradation curves of node stiffness as the loading displacement increases are plotted. By comparing the stiffness retention capacity of nodes with different structural parameters in the elastic, yielding, and failure stages, the influence of node design parameters on the stiffness degradation process is quantitatively analyzed. The stiffness degradation data obtained from the simulation is normalized, and the results are shown in Figure 3.

As can be seen from Figure 3(a), the initial level of nodal stiffness is relatively high. As more load is loaded, there is a strong decreasing tendency of the stiffness beyond the yield point and a slowing tendency of the stiffness decay beginning on entering into the failure stage. Figure 3(b), comparing the equivalent stiffness retention coefficients of the various nodal structures, reveals that the equivalent stiffness retention coefficient of the nodal with the optimized reinforcement and viable sleeve length is 0.82, which is an increment of about 15.49 per cent with respect to the bench nodal. This is primarily due to the fact that reasonable reinforcement configuration is better on the confinement of the core concrete and the propagation of cracks and crushing of the concrete as well as the stable transmission of force in the sleeve connection region that the nodal remains to give some contribution of the stiffness at the plastic stage. Before yielding, the stiffness degradation of the node is relatively small; after entering the plastic stage, the stiffness decay is closely related to the degree of damage accumulation in the core area.

NODAL DUCTILITY AND DEFORMATION CAPACITY

To evaluate the nonlinear deformation capacity and energy dissipation characteristics of prefabricated assembly structure connection nodes after exceeding the elastic stage, the yield displacement and ultimate displacement of each node model are determined using the energy equivalence method based on the load-displacement full-process curves obtained from finite element simulation, and the node ductility coefficients are calculated. By comparing the displacement ductility indices of nodes under different material strength grades and connection construction parameters, the influence of node design variables on the plastic deformation capacity of the structure is analyzed. The calculation results of the ductility coefficients of nodes with different parameters are summarized and organized, and the results are shown in Figure 4.

Figure 4(a) indicates that the nodal ductility coefficient of C30 concrete is 3.82, whereas that of C60 concrete is 3.47. Nodal ductile coefficient is inversely proportional to the concrete strength. The reason behind this phenomenon is more vivid brittle nature of the high-strength concrete that leads to accelerated rate of stress drop as soon as the peak stress is achieved and comparatively low amount of accumulated plastic deformation on the area in the core before crushing. Figure 4(b) indicates that nodal ductility coefficient to sleeve length of 180 mm is 3.71, which is about 12 percent more than a nodal with sleeve length of 120 mm. The extended sleeve length is used to increase the bond strength transfer length in between the reinforcing steel and concrete, enhancing the stress transfer path in the nodal area, and reducing the degrading process of bond between the reinforcing steel and concrete, so that the nodal area is able to sustain some deformation capacity even at the ultimate load.

COMPREHENSIVE SAFETY EVALUATION INDEX AND LEVEL DETERMINATION OF NODES

To quantitatively evaluate the overall safety performance of connection nodes in prefabricated assembled structures, the extracted load-bearing capacity margin, stiffness degradation coefficient, and ductility index are standardized based on the safety evaluation model. A weighted calculation is then performed to obtain the comprehensive safety evaluation index for each node model. The distribution patterns of the evaluation indices for nodes under different material strengths and structural parameters are compared, and the influence of node design variables on comprehensive safety performance is analyzed. The evaluation indices of each node are then categorized according to the safety level classification standards, as shown in Figure 5.

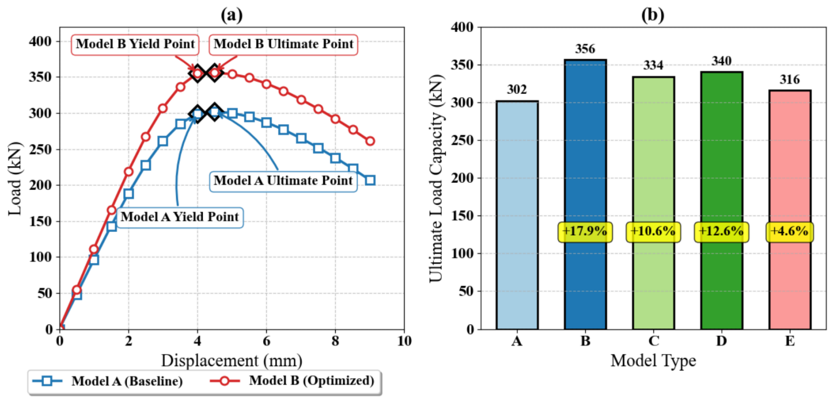

FIGURE 2. Evolution of node bearing capacity: (a) Load-displacement curve; (b) Comparison of ultimate bearing capacity

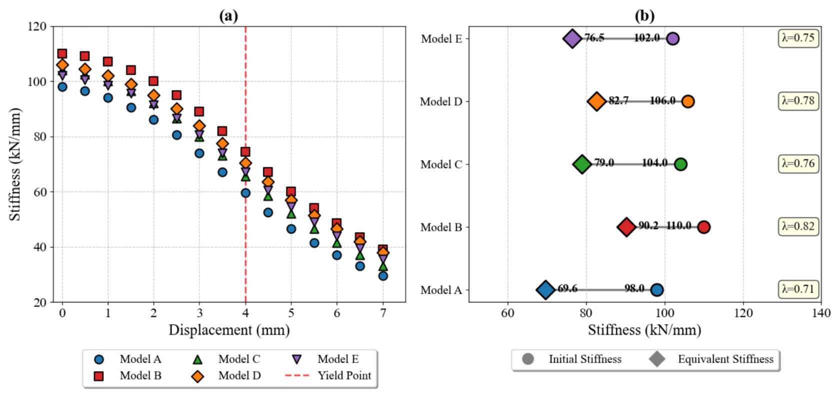

FIGURE 3. Nodal stiffness degradation curve: (a) Stiffness as a function of displacement curve; (b) Comparison of equivalent stiffness retention coefficients

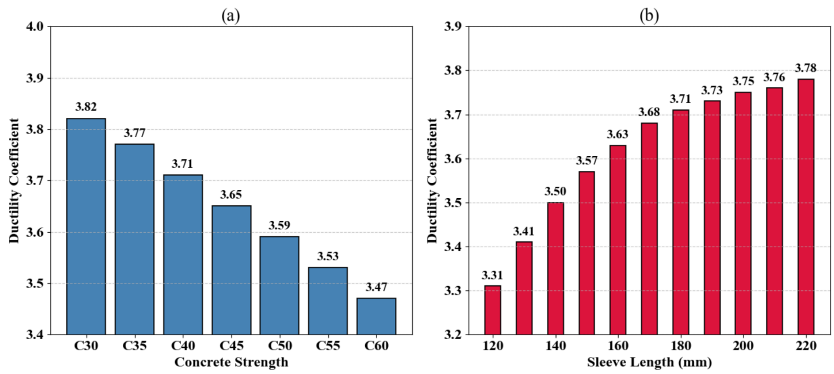

FIGURE 4. Calculation results of nodal ductility coefficient: (a) Comparison of nodal ductility coefficients for different concrete strengths; (b) Comparison of nodal ductility coefficients for different sleeve lengths

Figure 5(a) shows a comparison of comprehensive safety evaluation indices for nodes with different parameters. The node using C45 concrete and a sleeve length of 180 mm has an evaluation index of 0.91, while the node using C30 concrete and a sleeve length of 180 mm has an evaluation index of 0.87. The node using C60 concrete with the same sleeve length has an evaluation index of 0.85. The higher evaluation index of C45 concrete nodes stems from its superior balance between material strength and deformation capacity compared to C30 and C60 concrete. C30 concrete has relatively insufficient strength reserve, and the reduced ductility of C60 concrete affects its overall safety performance. The node with a sleeve length of 220 mm has a higher evaluation index than the node with a sleeve length of 120 mm, indicating that increasing the sleeve length improves the synergistic performance between the steel reinforcement and concrete, and reduces the stress concentration in the connection area. Figure 5(b) shows the

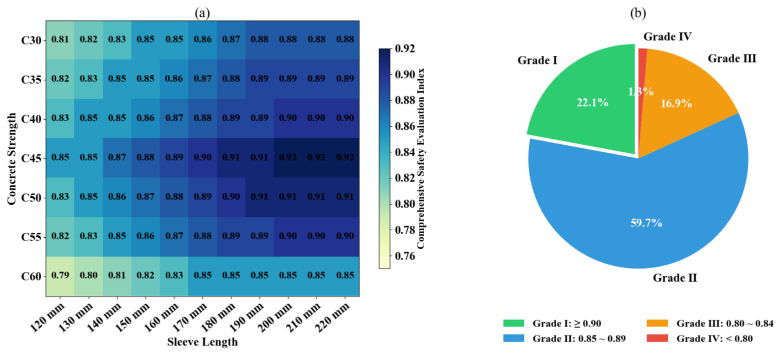

FIGURE 5. Comprehensive safety evaluation results of nodes: (a) Comparison of comprehensive safety evaluation indices for nodes with different parameters; (b) Distribution proportion of node safety levels (based on 100 nodes)

distribution of node safety levels, indicating that 81.8% of nodes have an evaluation index higher than 0.85, placing them in the higher safety level range. The comprehensive safety evaluation index of the nodes ranges from 0.79 to 0.92.

IV. CONCLUSION

The paper is developed as a framework and a mechanical model to analyze the stress mechanism of prefabricated assembled structural connection nodes, specifically incorporating technical architectures and fiber morphology as fundamental reinforcement parameters. By integrating the spatial distribution of yarns into the structural analysis, the proposed model provides a high-precision quantitative evaluation of load transfer and mechanical stability at the joint interfaces. Together with numerical simulation based on finite elements, it is a systematic study of the stress distribution, development of deformation and failure modes of nodes under various load conditions. The parameters of bearing capacity, stiffness evolution, and ductile parameters are key performance indicators that are taken out. It is based on this that a complete safety assessment system comprised of bearing capacity margin, stiffness degradation coefficient and deformation control indicators are implemented, and an outcome can be achieved to the scope of the quantitative measurement of structural performance of the node. Under C50 concrete, HRB500 and 180 mm sleeve, experimental results show the final bearing capacity of the node as 356 kN; the retention coefficient of the equivalent stiffness is 0.82; the coefficient of ductility is 3.59; the maximum safety assessment index is over 0.9. The research results demonstrate that this methodology effectively integrates technical architectures into the mechanical performance study and safety analysis of pre-assembled connection nodes, establishing a high-precision framework for structural joint design. By incorporating fiber morphology and the spatial distribution of yarns into the analytical model, the approach provides a systematic, multi-scale evaluation of the load-bearing stability and overall engineering safety of the node.

AUTHOR CONTRIBUTIONS

Jipeng Liu designed, collected and analyzed the data, and drafted the manuscript. Jipeng Liu conducted the study, critically revised the manuscript for important intellectual content, and gave final approval of the version to be published. Jipeng Liu participated fully in the work, take public responsibility for appropriate portions of the content, and agreed to be accountable for all aspects of the work in ensuring that questions related to the accuracy or integrity of any part of the work are appropriately investigated and resolved.

CONFLICTS OF INTEREST

The author declares no conflict of interest.

FUNDING

This work was supported by the Project Selected via Open Bidding, Science and Technology Program of Henan Provincial Department of Housing and Urban-Rural Development (Grant No.HNJS-2025-B4).

ACKNOWLEDGEMENTS

Not applicable.

REFERENCES

[1] X. Li, C. Wang, M. A. Kassem, H. H. Alhajlah, and S. Bimenyimana, “Evaluation method for quality risks of safety in prefabricated building construction using SEM-SDM approach,” International Journal of Environmental Research and Public Health, vol. 19, no. 9, pp. 5180-5187, 2022, doi: 10.3390/ijerph19095180.

[2] X. Li, R. Chen, W. Chen, and C. Y. Jim, “Safety-risk assessment system for prefabricated building construction in China,” Engineering, Construction and Architectural Management, vol. 32, no. 12, pp. 8073-8096, 2025, doi: 10.1108/ECAM-03-2024-0287.

[3] C. Yang, B. Xu, J. Xia, H. Chang, X. Chen, and R. Ma, “Mechanical behaviors of inter-module connections and assembled joints in modular steel buildings: a comprehensive review,” Buildings, vol. 13, no. 7, pp. 1727-1734, 2023, doi: 10.3390/buildings13071727.

[4] R. Chang, N. Zhang, and Q. Gu, “A review on mechanical and structural performances of precast concrete buildings,” Buildings, vol. 13, no. 7, pp. 1575-1582, 2023, doi: 10.3390/buildings13071575.

[5] Z. Zhu, F. Wu, and J. Hao, “Mechanical behavior of a novel precast concrete beam-column joint using the mortise-tenon connection,” Sustainability, vol. 15, no. 19, pp. 14586-14592, 2023, doi: 10.3390/su151914586.

[6] M. Guan, J. Xiao, Y. Wang, Y. Zhang, Z. Liang, and Z. Lai, “Seismic behavior of innovative precast hybrid steel reinforced concrete beam-column connections,” Journal of Constructional Steel Research, vol. 203, no. 1, pp. 107817-107825, 2023, doi: 10.1016/j.jcsr.2023.107817.

[7] G. Hu, Z. Zhang, B. Cao, Z. Pan, and L. Zeng, “Seismic behavior of precast concrete beam-column joints with bending moment-shear separation controllable plastic hinge,” Engineering Structures, vol. 304, no. 1, pp. 117585-117592, 2024, doi: 10.1016/j.engstruct.2024.117585.

[8] R. Zhang, Y. Zhang, A. Li, and T. Y. Yang, “Experimental study on a new type of precast beam-column joint,” Journal of Building Engineering, vol. 51, no. 1, pp. 104252-104259, 2022, doi: 10.1016/j.jobe.2022.104252.

[9] L. Chen, J. Feng, Y. Xue, and C. Liang, “Seismic behavior of an innovative prefabricated steel-concrete composite beam-column joint,” Journal of Building Engineering, vol. 76, no. 1, pp. 107211-107218, 2023, doi: 10.1016/j.jobe.2023.107211.

[10] E. F. Deng, J. Y. Lian, Z. Zhang, H. Qian, G. C. Zhang, P. Zhang, et al., “Axial mechanical behavior of an innovative liftable connection for modular steel construction,” Thin-Walled Structures, vol. 182, pp. 110256-110262, 2023, doi: 10.1016/j.tws.2022.110256.

[11] S. Xiao and N. I. Fomin, “Development and systematic review of connection techniques for RC Precast structural elements: Beam and Column Connection,” Heliyon, vol. 10, no. 16, Art. no. e35886-e35904, 2024, doi: 10.1016/j.heliyon.2024.e35886.

[12] A. L. Zhang, X. D. Chen, Y. X. Zhang, X. Zhao, and W. Z. Huang, “Experimental and theoretical investigation of prefabricated separated core tube flange column connection joint,” Journal of Constructional Steel Research, vol. 201, no. 1, pp. 107694-107700, 2023, doi: 10.1016/j.jcsr.2022.107694.

[13] X. Pang and Y. Li, “Seismic performance evaluation of precast post-tensioned high-performance concrete frame beam-column joint under cyclic loading,” Scientific Reports, vol. 14, no. 1, pp. 12327-12342, 2024, doi: 10.1038/s41598-024-63083-y.

[14] Y. Helal, R. Garcia, T. Imjai, P. Aosai, M. Guadagnini, and K. Pilakoutas, “Seismic behaviour of Exterior RC beam-column joints repaired and strengthened using post-tensioned metal straps,” Bulletin of Earthquake Engineering, vol. 22, no. 6, pp. 3261-3286, 2024, doi: 10.1007/s10518-024-01904-1.

[15] X. Hu, W. Xue, and Y. Lv, “Experimental studies on structural performance of precast concrete shear walls with innovative UHPC-based connections,” Journal of Building Engineering, vol. 73, no. 1, pp. 106748-106755, 2023, doi: 10.1016/j.jobe.2023.106748.

[16] D. Kim and H. Ju, “Shear Strength Evaluation of Precast Concrete Beam-Column Joints Considering Key Influencing Parameters,” Sustainability, vol. 18, no. 1, pp. 468-475, 2026, doi: 10.3390/su18010468.

[17] L. Chen, Z. Wang, B. Ma, G. Peng, C. Wang, and L. Zhou, “Seismic performance of a novel steel-concrete composite beam-column joint,” Journal of Constructional Steel Research, vol. 229, no. 1, pp. 109479-109486, 2025, doi: 10.1016/j.jcsr.2025.109479.

[18] Y. Xiao, M. Yu, and W. Liu, “Finite Element Analysis of Prefabricated Semi-Rigid Concrete Beam-Column Joint with Steel Connections,” Applied Sciences, vol. 14, no. 12, pp. 5070-5077, 2024, doi: 10.3390/app14125070.

[19] J. Zheng, Z. Pan, H. Zhen, X. Deng, C. Zheng, and Z. Qiu, “Experimental investigation on the seismic behavior of precast concrete beam-column joints with five-spiral stirrups,” Buildings, vol. 13, no. 9, pp. 2357-2364, 2023, doi: 10.3390/buildings13092357.

[20] M. L. Zhuang, J. Cheng, D. Fei, C. Sun, Z. Wang, B. Chen, et al., “Numerical Simulation Study on the Seismic Performance of Prefabricated Fiber-Reinforced Concrete Beam-Column Joints With Grouted Sleeve Connections,” International Journal of Concrete Structures and Materials, vol. 18, no. 1, pp. 26-41, 2024, doi: 10.1186/s40069-024-00671-2.

[21] M. Ebadi-Jamkhaneh, D. P. N. Kontoni, and A. H. Ebrahimi, “Assessment of different methods for enhancing progressive collapse resistance of irregular reinforced concrete buildings using pushdown analysis,” Arabian Journal for Science and Engineering, vol. 49, no. 10, pp. 13861-13883, 2024, doi: 10.1007/s13369-024-08847-4.

[22] U. A. Noor, M. A. Jadoon, K. Onyelowe, A. Shahzad, K. Ghaedi, and H. Alabduljabbar, “Non-linear finite element analysis of SFRC beam-column joints under cyclic loading: enhancing ductility and structural integrity,” Scientific Reports, vol. 14, no. 1, pp. 18152-18183, 2024, doi: 10.1038/s41598-024-69270-1.

[23] A. Hamoda, G. Elsamak, M. Emara, M. Ahmed, and Q. Q. Liang, “Experimental and numerical studies of reinforced concrete beam-to-steel column composite joints subjected to torsional moment,” Engineering Structures, vol. 275, no. 1, pp. 115219-115226, 2023, doi: 10.1016/j.engstruct.2022.115219.

[24] L. Chen, X. Qiang, X. Jiang, and J. Bai, “Numerical study of steel-concrete composite beams strengthened by CFRP plates with prestressed unbonded reinforcement system,” Engineering Failure Analysis, vol. 157, no. 1, pp. 107905-107912, 2024, doi: 10.1016/j.engfailanal.2023.107905.

[25] W. Mansour, M. Ghalla, W. Li, P. Wang, M. Badawi, and A. Albogami, “Evaluation of the axial compressive response of reinforced concrete brick columns externally wrapped with stainless steel sheets: experimental and numerical analysis,” Construction and Building Materials, vol. 490, no. 1, pp. 142501-142508, 2025, doi: 10.1016/j.conbuildmat.2025.142501.

[26] Z. Wang, J. Zhao, X. Chen, S. Liu, and B. Ma, “Experimental investigation of seismic response of precast concrete panels with castellated keys support pillar connections under in-plane cyclic loading,” Scientific Reports, vol. 13, no. 1, pp. 21764-21785, 2023, doi: 10.1038/s41598-023-35386-z.

[27] W. Yin, Y. Chang, and E. Xiong, “Research on the Mechanical Performance of Ultra-High Performance Concrete Reinforced Truss Precast Slabs during the Construction Phase,” International of Civil Engineering, vol. 24, no. 1, pp. 89-100, 2026, doi: 10.1007/s40999-025-01173-2.

[28] M. D’Aniello, R. Montuori, E. Nastri, V. Piluso, and P. Todisco, “Parametric Finite Element Study on FREEDAM Beam to Column Joints with Different Details of the Haunch Slotted Holes,” Applied Sciences, vol. 14, no. 7, pp. 2770-2776, 2024, doi: 10.3390/app14072770.

[29] W. Li, H. Ye, H. Liu, and B. Chen, “Development and testing of demountable RC column-to-steel beam connections under cyclic loading,” Soil Dynamics and Earthquake Engineering, vol. 159, no. 1, pp. 107342-107348, 2022, doi: 10.1016/j.soildyn.2022.107342.

[30] C. Wang, R. Liu, X. Wang, et al., “Review of the Rearch on the Imapct Resistance Mechanical Performance of Prestressed Segmental Precast and Assembled Piers,” Structural Durability & Health Monitoring, pp. 1-10, 2025, doi: 10.32604/sdhm.2025.060580.

[31] W. K. Hong, T. D. Pham, D. H. Nguyen, T. A. Le, M. C. Nguyen, and V. T. Nguyen, “Experimental and nonlinear finite element analysis for post-tensioned precast frames with mechanical joints,” Journal of Asian Architecture and Building Engineering, vol. 22, no. 5, pp. 2922-2945, 2023, doi: 10.1080/13467581.2023.2171733.

[32] Z. Xiong, Y. Lin, Q. Wang, W. Yang, C. Shen, and J. Zhang, “Research on safety performance evaluation and improvement path of prefabricated building construction based on DEMATEL and NK,” Applied Sciences, vol. 14, no. 17, pp. 8010-8017, 2024, doi: 10.3390/app14178010.

[33] M. Cai, H. Zhu, Q. Chen, T. Rabczuk, and X. Zhuang, “Mechanical behavior of ultra-high toughness concrete (UHTC) tunnel segmental joints,” Tunnelling and Underground Space Technology, vol. 151, no. 1, pp. 105838-105844, 2024, doi: 10.1016/j.tust.2024.105838.

[34] Y. E. Kim, J. Park, Q. B. To, K. Lee, and J. Shin, “Finite element analysis-based blast performance evaluation for reinforced concrete columns with shear and flexure failure modes,” Sustainability, vol. 15, no. 20, pp. 14967-14974, 2023, doi: 10.3390/su152014967.

[35] L. Q. Zheng, X. Y. Chen, C. G. Wei, and G. Y. Yan, “Seismic performance of prefabricated beam-to-column joint with replaceable energy-dissipating steel hinge,” Bulletin of Earthquake Engineering, vol. 20, no. 3, pp. 1865-1895, 2022, doi: 10.1007/s10518-021-01310-x.